nature

International weekly journal of science

Volume 404 No. 6781 27 April 2000

Recycled oceanic crust observed in 'ghost plagioclase' within the source of Mauna Loa lavas

Alexander V. Sobolev, Albrecht W. Hofmann & Igor K. Nikogosian

Recycled oceanic crust observed in 'ghost plagioclase' within the source of Mauna Loa lavas

Alexander V. Sobolev*†, Albrecht W. Hofmann* & Igor K. Nikogosian*‡†

** Max-Planck-Institut für Chemie, Postfach 3060, 55020 Mainz, Germany*
† Vernadsky Institute of Geochemistry, Russian Academy of Sciences, Kosygin Street 19, 117975 Moscow, Russia
‡ Department of Petrology, Vrije Universiteit, De Boelelaan 1085, 1081 HV, Amsterdam, The Netherlands

The hypothesis that mantle plumes contain recycled oceanic crust[1] is now widely accepted. Some specific source components of the Hawaiian plume have been inferred to represent recycled oceanic basalts[2], pelagic sediments[3,4] or oceanic gabbros[5]. Bulk lava compositions, however, retain the specific trace-element fingerprint of the original crustal component in only a highly attenuated form. Here we report the discovery of exotic, strontium-enriched melt inclusions in Mauna Loa olivines. Their complete trace-element patterns strongly resemble those of layered gabbros found in ophiolites, which are characterized by cumulus plagioclase with very high strontium abundances[6]. The major-element compositions of these melts indicate that their composition cannot be the result of the assimilation of present-day oceanic crust through which the melts have travelled. Instead, the gabbro has been transformed into a (high-pressure) eclogite by subduction and recycling, and this eclogite has then been incorporated into the Hawaiian mantle plume. The trace-element signature of the original plagioclase is present only as a 'ghost' signature, which permits specific identification of the recycled rock type. The 'ghost plagioclase' trace-element signature demonstrates that the former gabbro can retain much of its original chemical identity through the convective cycle without completely mixing with other portions of the former oceanic crust.

We studied melt inclusions in olivine phenocrysts in three lavas covering 50 kyr of eruption history of Mauna Loa volcano, Hawaii. The lavas are picrites with more than 20% olivine phenocrysts. We examined 250 melt inclusions by electron microprobe, and selected 160 of these for ion microprobe analysis. All measured compositions were corrected for Fe–Mg exchange between included melt and host olivine, and for crystallization of olivine on the cavity walls (see Methods). They are believed to represent the primary compositions of entrapped melts.

The corrected major-element compositions of the melt inclusions are similar to primitive Mauna Loa lavas, and show the olivine control characteristics typical of Hawaiian tholeiites (Fig. 1). This observation and numerical simulation of plagioclase melting using mineral-melt geothermometry[7] suggest that all reconstructed trapped melts are well within the olivine crystallization field at low pressures and are considerably undersaturated with respect to plagioclase at any pressure of its stability (Fig. 1).

The melt inclusions show significant variations in their incompatible-trace-element concentrations. We distinguish two groups of melts on the basis of Sr concentration and Sr/REE ratio (Figs 2 and 3; REE, rare-earth element). Most of the melt inclusions show moderate enrichment of Sr relative to Ce, and will be referred to as 'normal'. Six inclusions show extreme Sr excess, and will be called 'Sr-rich'.

The average trace-element composition of the inclusions is remarkably similar to the Mauna Loa lavas (Fig. 2a)[5]. However, the range of incompatible element (for example, light-REE, Ba, Th) concentrations and ratios is much greater than is found in Hawaiian

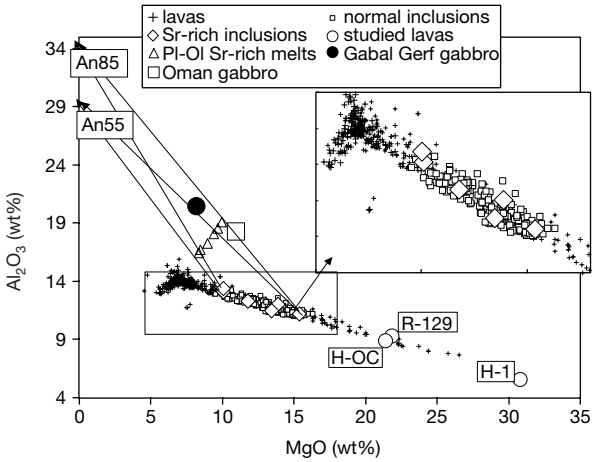

Figure 1 Al_2O_3 versus MgO in lavas and inclusions. The figure shows data for Mauna Loa lavas (see GEOROC database at http://georoc.mpch-mainz.gwdg.de), corrected normal and Sr-rich melt inclusions, bulk compositions of the three investigated lava samples (with sample numbers), and average compositions of ophiolite gabbros from Gabal Gerf[6] and Oman (C. J. Garrido & P. B. Kelemen, manuscript in preparation). The open triangles show Sr-rich melts saturated in plagioclase and olivine, calculated by PETROLOG software[7] (see Supplementary Information). Arrows show assimilation trends of plagioclase with different anorthite contents (An in mol%). The apparent olivine control trend is similar for all inclusion types and lavas. All lavas with MgO > 7% and all inclusions are plagioclase-undersaturated. Sr-rich inclusions follow the olivine control trend, and show no sign of Al enrichment resulting from interaction of melt with gabbro or plagioclase.

tholeiitic lavas. This is illustrated in Fig. 3, where $(La/Sm)_n$ (here subscript n means normalization to the composition of primitive mantle[30]) is used as a measure of the relative depletion or enrichment of incompatible elements. In normal inclusions, $(La/Sm)_n$ varies from 0.3 to 1.9, whereas Mauna Loa lavas[8] show a much narrower range of 1.0–1.6.

Less than 4% of the inclusions are Sr-rich. Compared with normal inclusions and Mauna Loa lavas, Sr-rich melts are also severely depleted in the most incompatible elements (Ba, Th, Nb, K, La, Ce, Nd and Zr). In contrast to the exotic incompatible-element signatures, heavy-REE and major-element compositions of these melts are typical for Mauna Loa lavas (Figs 1 and 3; Tables 1 and 2 in Supplementary Information). Two features of the heavy-REE distributions, their relative depletion and their low variability (within analytical error), indicate that garnet was in equilibrium with both normal and Sr-rich melts.

In most of the olivine grains, the composition of the melt inclusions is fairly uniform. This has been demonstrated by closely spaced, sequential thin-sectioning, which yielded up to 21 separate inclusions in 6 sections of a single olivine grain. However, the exotic melt inclusions with either high Sr/Ce or extreme La/Sm ratios are invariably associated with normal inclusions in the same grain. The most extreme example is olivine grain HOC-76. Here, the concentrations of Ba, Nb and K differ by a factor of more than 10 in melt inclusions separated by a few hundred micrometres of host olivine (see Fig. 5 and Table 1 in Supplementary Information). Four coexisting inclusions are normal with respect to Sr, but variably depleted in the most incompatible elements, with one inclusion of ultra-depleted type. The fifth inclusion is Sr-rich.

These observations show that the exotic melt fractions are very small in volume and are therefore readily 'lost' in the bulk magmas by mixing processes during the residence time of single olivine crystals. Similar relationships were also found in mid-ocean-ridge basalt (MORB)[9,10]; they thus appear to be general features of mantle-derived magmas.

Melt inclusions with significant excess of Sr and Ba have been found also on Iceland[11] and mid-ocean ridges[12]. They have been interpreted as a result of melting of plagioclase-bearing mantle

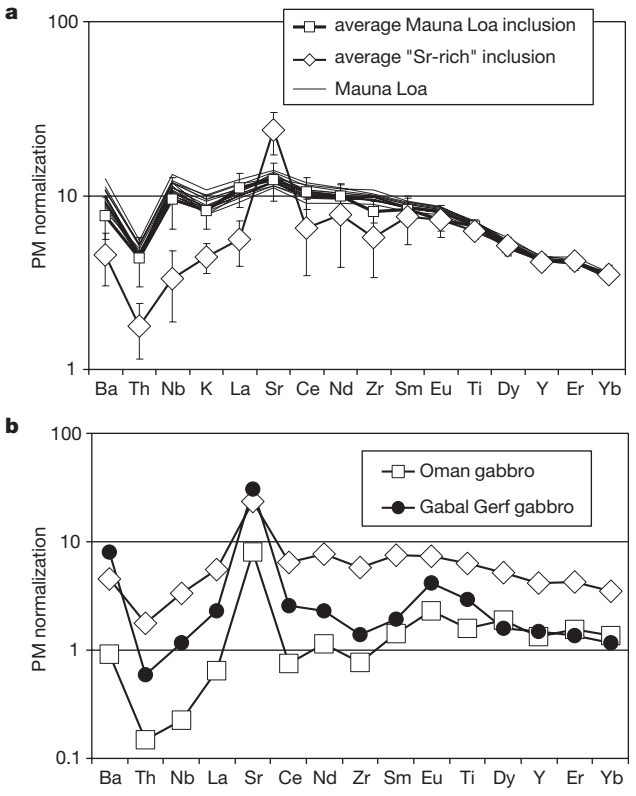

Figure 2 Incompatible-element patterns in melt inclusions, lavas and ophiolitic gabbros normalized to the composition of primitive mantle (PM)[30]. **a,** Average incompatible-element patterns of normal and Sr-rich melt inclusions in olivine phenocrysts and lavas of Mauna Loa (Hawaii). Error bars represent one standard deviation. The compositions of 15 historical and prehistoric Mauna Loa lavas analysed by isotope dilution mass spectrometry and X-ray fluorescence spectrometry techniques are shown for comparison (A.W.H. *et al.*, unpublished data). Inclusion compositions were reconstructed up to equilibrium with the most Mg-rich olivine (Fo 90.8) indicated in Mauna Loa section of HSDP pilot hole[31]. This leads to 17 ± 0.5 wt% MgO in the melt. Lava compositions were recalculated to 17 wt% MgO using the olivine control line from Fig. 1. **b,** Comparison of incompatible-element patterns in Sr-rich melt inclusions and ophiolitic gabbros. The specific features of Sr-rich inclusions, namely strong Sr positive anomaly, strong negative Th, Nb and Zr anomalies, as well as a moderate positive Ba anomaly, mimic those of gabbros from Oman (C. J. Garrido & P. B. Kelemen, manuscript in preparation) and Gabal Gerf[6]. In gabbros these features are caused by accumulation of plagioclase. The amplitudes of extremes in the incompatible-element patterns of Sr-rich melt inclusions and gabbros are remarkably similar. An exception is the apparent absence of a positive Eu anomaly in melts. This feature is not surprising, partly because a source Sm/Eu ratio will be increased during melting in the presence of garnet (see Supplementary Information) and partly because the expected Eu anomaly (assuming Eu*/Sr* = 0.05–0.1) is equal to or less than the analytical error of about 20% (see Methods). $Eu^* = \frac{Eu_n}{Sm_n + Gd_n} - 1$; $Sr^* = \frac{Sr_n}{Ce_n} - 1$.

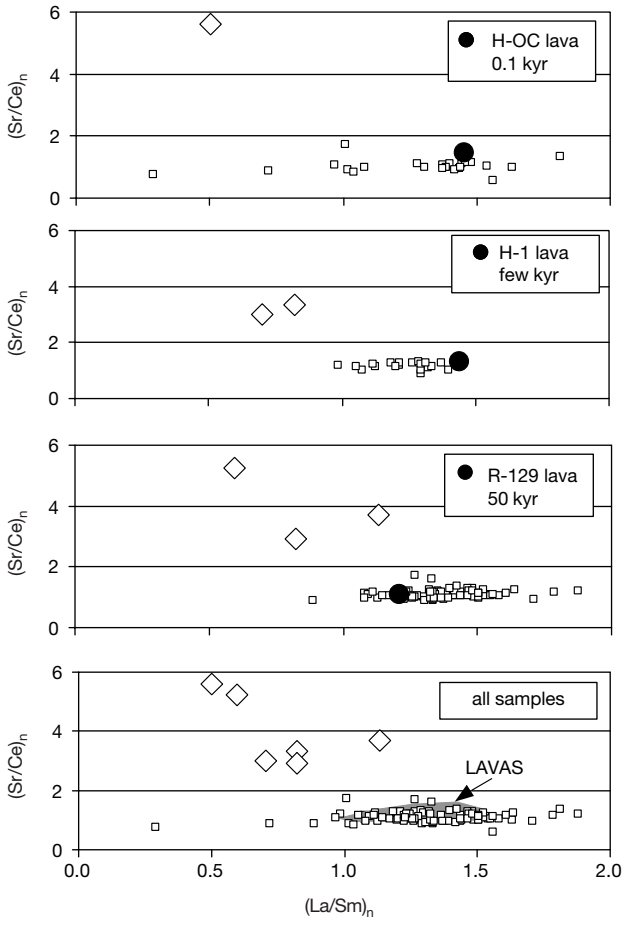

Figure 3 Sr/Ce versus La/Sm ratios of melt inclusions in olivine and host lavas, normalized to primitive mantle values[30]. Sr-rich melts are present in all three samples. The range of La/Sm ratios of inclusions far exceed those for lavas (ref. 8 and the GEOROC database, see Fig. 1 legend). Furthermore, there is no relationship between the La/Sm ratios of host rocks and melt inclusions: all inclusions of sample H-1 and most inclusions of H-OC are more depleted in La than the host lavas, while the reverse is true for sample R129. This demonstrates that the olivines were not crystallized directly from the melt that transported them at the time of eruption.

sources[11,12]. This mechanism, irrespective of its merits in the case of Iceland or MORB, is clearly not applicable to melt production beneath Hawaii, which occurs largely, if not completely, in the garnet peridotite facies (see, for example, refs 5, 13).

The incompatible-element patterns of Sr-rich melts are characteristic of oceanic-crust gabbroic rocks enriched in cumulus plagioclase (Fig. 2b). In contrast, the major-element compositions of corrected Sr-rich inclusions are similar to normal inclusions and lavas, and show no enrichment in Al such as would result from assimilation of plagioclase or plagioclase-rich gabbro (Fig. 1). However, the comparison of absolute concentrations of elements in corrected Sr-rich and normal inclusions is subject to the assumption of equal and known initial FeO contents, an assumption which is fundamental to the correction procedure (see Methods). Because the compositions of the Sr-rich melts are unique, this assumption cannot easily be proved for them. Nevertheless, Fig. 4 shows that major-element ratios, such as Al/Ca or Al/Ti, which are not affected either by the correction procedure or by fractional crystallization of olivine, are indistinguishable for Sr-rich and normal melts. At the same time, the relative Sr content varies by up to a factor of 5 between the two groups.

In order to produce such extreme Sr enrichments in the melt by assimilation-type processes or reactive porous flow in the crust, at least 60% of Sr-rich gabbro or 40% of plagioclase would have to be consumed (see Fig. 4 and Supplementary Information). This would drastically affect relative Al concentrations, which is clearly not observed (Figs 1 and 4). This is strong evidence against the production of Sr-rich melts by direct reaction with plagioclase-bearing rocks. (Carbonatites also possess high Sr concentrations, but can be ruled out because, unlike the Sr-rich inclusions, they also have high Ba, light-REE and Th contents[14]). We therefore conclude that the anomalous compositions are inherited from the source of the melts and represent recycled gabbro.

The fate of subducted oceanic lithosphere is not well understood. In particular, it has not been clear to what extent former crust can retain its "chemical identity" in a plume source[15]. Here we assume that the crustal component has not been completely mixed with the peridotitic matrix but retained a separate identity, thus forming a "marble cake" mantle[16]. At high pressures, crustal gabbro transforms to eclogite (garnet–clinopyroxene–SiO_2 ± kyanite ± rutile)[17]. Eclogites with similar Sr anomalies have indeed been observed in mantle xenoliths[18].

How does such an eclogite-bearing "marble cake" melt? Experimental studies[19,20] predict that eclogite bodies containing containing coesite, will start to melt at higher pressures than the ultramafic matrix in an ascending plume. The resulting (Si-rich) melt will infiltrate the surrounding peridotite, react with it to form pyroxene, and modify the composition of garnet[20]. Thus, the incompatible-element signature of the recycled crust is transferred to the ascending ultramafic source before the latter starts to melt. Subsequent adiabatic melting of such peridotites in the garnet stability field will then produce melts characterized by a ghost plagioclase signature, while residual garnet still buffers Al and heavy-REE at low abundances (see Supplementary Information). This is exactly what distinguishes the composition of the Sr-rich melts.

We emphasize that, because of the incompatible nature of the ghost plagioclase signature, even small amounts (down to 3 wt%) of partial melt originating in the eclogite could produce large geochemical effects without significant change in mineral compositions and proportions in the metasomatized peridotite (see Supplementary Information). This implies that major-element compositions of melts formed in adjacent metasomatized and normal peridotites will be similar.

In this context we note that a low $\delta^{18}O$ signature, as observed for example in olivines from Mauna Kea[21], is not a necessary criterion for former or present gabbro to be involved in magma generation. This is partly because oxygen is a major element and its isotopic composition will not necessarily change significantly in the process discussed above. Moreover, oceanic gabbros do not universally possess such a signature[22]. For example, the Wadi Hilti gabbro profile of the Oman ophiolite[22], and most gabbros drilled in site 735 in actual oceanic crust[23], are essentially normal in $\delta^{18}O$. The absence of such a signature in Mauna Loa olivines[21] can therefore not be construed as evidence against the presence of a gabbroic fingerprint.

Why do normal melt inclusions and lavas have higher incompatible-element concentrations than Sr-rich melts? We suggest that their mantle source is also affected by recycled crust, but this crustal component is closer to average oceanic crust than cumulus-plagioclase-rich, incompatible-element-depleted gabbro. We therefore visualize the plume source as a mixture of peridotite enriched in components of recycled oceanic crust, only one of which is plagioclase-rich gabbro. The accumulation of plagioclase is a result of crystal settling during fractional crystallization. This limits the spatial scale of such heterogeneities to a maximum of a few kilometres or even less, if the data on oceanic gabbros of Hart *et al.*[23] are representative of lower oceanic crust. Mixing these local heterogeneities with the rest of the oceanic crust would erase the ghost plagioclase signature. Thus, our results suggest that such

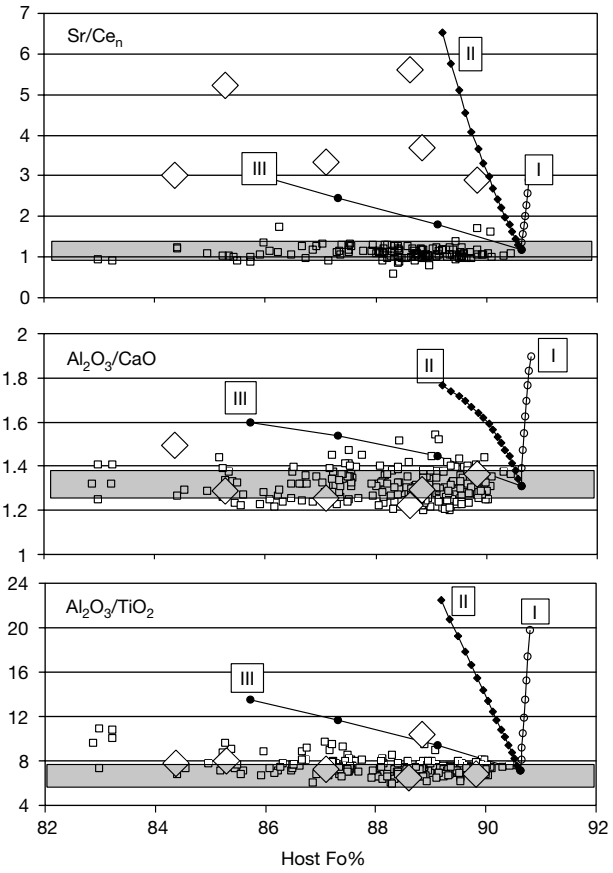

Figure 4 Sr/Ce, Al_2O_3/CaO and Al_2O_3/TiO_2 ratios in melt inclusions versus forsterite content of host olivine. Shaded areas show ranges of lava compositions from GEOROC database (see Fig. 1 legend). Note that Sr-rich melts were trapped by the olivines in nearly the entire range of their composition. The numbered curves show the effects of assimilation of plagioclase from Gabal Gerf gabbro (model I: up to 40 wt% assimilation), assimilation of Gabal Gerf gabbro (model II: up to 80 wt% assimilation) and of assimilation-fractional-crystallization processes (model III: up to 60 wt% assimilated gabbro and 15% olivine fractionation) (see Supplementary Information). The results show that interaction with gabbro sufficient to increase Sr/Ce ratios to levels observed in Sr-rich inclusions would require large and correlated effects on Al/Ca and Al/Ti ratios, none of which is observed in the Sr-rich inclusions.

mixing is incomplete at best, and that some local heterogeneities do survive the entire recycling process.

In contrast with the source heterogeneity required to produce Sr-rich melts, the extreme fractionation between elements with different incompatibility—demonstrated by La/Sm in Fig. 3 for the normal melts—can be produced by the melting process itself. This requires a melting process with efficient extraction of small melt fractions of less than 2 wt% for classical mantle plumes, similar to mid-oceanic ridges[9].

The extreme heterogeneity of the trace-element patterns requires that some melts preserve the source heterogeneities up to the point where they are incorporated into the olivine phenocrysts. Because the olivines crystallized at low pressure (see Methods), this appears to take place in crustal magma chambers, and therefore small, compositionally distinct magma batches must be transported from mantle to crust, perhaps through separate channels arranged in "fractal trees"[24]. The much greater homogeneity of the erupted Mauna Loa lavas is the result of subsequent mixing processes[25]. □

Methods

Samples

The studied historic (1868) H-OC and prehistoric H-1 samples were described in detail elsewhere[13]. Sample R129-8.1 came from 210 m depth (unit 32) of the pilot hole of the Hawaii Scientific Drilling Project (HSDP)[26] and has been dated at approximately 50 kyr (ref. 27). Olivines were separated from samples H-OC and H-1 by hand-picking from coarse fragments (0.5–1 mm) of lava samples crushed by hand. Sample R129-8.1 was sequentially sectioned, and olivines were picked directly from doubly polished 'thick sections' (200–300 μm thick). This rules out the possibility that olivines with exotic melt inclusions might be introduced by sample contamination.

Inclusions

Melt inclusions in olivine from H-OC and H-1 samples were crystallized as aggregates of clinopyroxene and glass. In order to reconstruct original compositions of trapped melt, these inclusions were heated on an optical heating stage until homogenization and were subsequently quenched[13].

Most inclusions in olivine from sample R129-8.1 are present as fresh glass with shrinkage bubbles, indicating crystallization of host olivine on the walls of the cavity[28]. Secondary alteration products are present in cracks but do not affect the main part of the inclusions, which consist of optically clear glass. The Sr-rich melts are not affected by secondary alteration, which is demonstrated by their low K and H_2O contents in addition to the optical observations (see Supplementary Information Table 1). No plagioclase has been observed either as a phase in melt inclusions or as phenocrysts or inclusions in olivine in all studied samples.

The pressure of entrapment of melt inclusions of both normal and exotic types is believed to be around 1 kbar. This conclusion is based on the following arguments: (1) melt inclusions commonly coexist with low-density CO_2-rich fluid inclusions corresponding to entrapment pressures of up to 1.3 kbar and partial H_2O pressures of 5–20 bar (ref. 13). Although there were no fluid inclusions found directly in association with exotic melt inclusions, their H_2O contents (0.2–0.3 wt%) fit the latter pressures. (2) The host olivines for all inclusions correspond to the high-Ca (CaO = 0.2–0.25 wt%) low-pressure variety[13]. (3) Optical heating experiments with exotic melt inclusions (olivine grains H-1-27, H-1-II/70 and HOC-76; see Supplementary Information Table 1) and normal inclusions lead to their homogenization without decrepitation which would be expected if internal pressures exceeded 3–5 kbar in large inclusions (more than 30 μm in diameter) in olivine[13,28]. (4) Exotic and normal melt inclusions coexist in single olivine grains.

Electron microprobe analysis

Inclusions and host olivine were studied by the Jeol Superprobe electron probe at the Department of Earth Sciences, Mainz University.

Ion microprobe analysis

Inclusions were analysed by ion microprobe ims-4f (Cameca) at the Institute of Microelectronics, Russian Academy of Science (Yaroslavl, Russia) using methods presented elsewhere[10]. In order to improve beam stability and avoid mass superposition, we used O^{2-} instead of O^- as a primary beam and a 100 kV high voltage offset. The resulting precision, as checked by standards (analysed as unknowns) is better than 10% relative for most elements, and around 20% relative for Eu (due to mass superposition with BaO) and Th where contents are below 0.50 p.p.m. In order to avoid problems caused by boundary layer effects in small inclusions[28], only relatively large melt inclusions with minimum dimensions of more than 30 μm were studied.

Reconstruction of composition of inclusions

All natural glassy inclusions in sample R129-8.1 show evidence of quenched olivine crystallization on the cavity walls. An attempt to remove this effect by 'reversing' this crystallization back to equilibrium with the host olivine[9] leads, however, to unrealistically low FeO in the melts compared with lavas. Moreover, the FeO contents in the glass are positively correlated with inclusion sizes. This effect is caused by the continued exchange of Fe–Mg between included melt and host olivine in response to the cooling of the magmatic system in equilibrium with constant olivine composition[29]. In order to remove this effect, the correction procedure as described by Danyushevsky *et al.*[29] was applied for all inclusions, assuming a uniform initial FeO content of 11.2 wt% for all melts (corresponding to the average value of primitive Mauna Loa lavas; see GEOROC database at http://georoc.mpch-mainz.gwdg.de) and equilibrium with host olivine at an oxygen fugacity corresponding to quartz–fayalite–magnetite buffer[13]. Trace-element concentrations in olivine were assumed to be zero.

Received 12 August 1999; accepted 15 March 2000.

1. Hofmann, A. W. & White, W. M. Mantle plumes from ancient oceanic crust. *Earth Planet. Sci. Lett.* **57,** 421–436 (1982).
2. Lassiter, J. C. & Hauri, E. H. Osmium-isotope variations in Hawaiian lavas: Evidence for recycled oceanic lithosphere in the Hawaiian plume. *Earth Planet. Sci. Lett.* **164,** 483–496 (1998).
3. Hauri, E. H. Major element variability in the Hawaiian mantle plume. *Nature* **382,** 415–419 (1996).
4. Blichert-Toft, J., Frey, F. A. & Albarede, F. Hf isotope evidence for pelagic sediments in the source of Hawaiian basalts. *Science* **285,** 879–882 (1999).
5. Hofmann, A. W. & Jochum, K. P. Source characteristics derived from very incompatible trace elements in Mauna Loa and Mauna Kea basalts, Hawaiian Scientific Drilling Project. *J. Geophys. Res.* **101,** 11831–11839 (1996).
6. Zimmer, M., Kröner, A., Jochum, K. P., Reischmann, T. & Todt, W. The Gabal Gerf complex: A Precambrian N-MORB ophiolite in the Nubian Shield, NE Africa. *Chem. Geol.* **123,** 29–51 (1995).
7. Danyushevsky, L. V. The effect of small amounts of H_2O on fractionation of mid-ocean ridge magmas. *Eos* **79** (suppl.), S375 (1998).
8. Rhodes, J. M. & Hart, S. R. in *Mauna Loa Revealed: Structure, Composition, History And Hazards* (eds Rhodes, J. M. & Lockwood, J. P.) 263–288 (Geophysical Monograph No. 92, American Geophysical Union, Washington, DC, 1995).
9. Sobolev, A. V. & Shimizu, N. Ultra-depleted primary melt included in an olivine from the Mid-Atlantic Ridge. *Nature* **363,** 151–154 (1993).
10. Sobolev, A. V. Melt inclusions in minerals as a source of principal petrological information. *Petrology* **4,** 209–220 (1996).
11. Gurenko, A. A. & Chaussidon, M. Enriched and depleted primitive melts included in olivine from Icelandic tholeiites - origin by continuous melting of a single mantle column. *Geochim. Cosmochim. Acta* **59,** 2905–2917 (1995).
12. Kamenetsky, V. S. *et al.* Calcic melt inclusions in primitive olivine at 43 degrees N MAR: evidence for melt-rock reaction/melting involving clinopyroxene-rich lithologies during MORB generation. *Earth Planet. Sci. Lett.* **160,** 115–132 (1998).
13. Sobolev, A. V. & Nikogosian, I. K. Petrology of long-lived mantle plume magmatism: Hawaii (Pacific) and Reunion Island (Indian Ocean). *Petrology* **2,** 111–144 (1994).
14. Veksler, I. V., Petibon, C., Jenner, G. A., Dorfman, A. M. & Dingwell, D. B. Trace element partitioning in immiscible silicate-carbonate liquid systems: an initial experimental study using a centrifuge autoclave. *J. Petrol.* **39,** 2095–2104 (1998).
15. Christensen, U. R. & Hofmann, A. W. Segregation of subducted oceanic crust in the convecting mantle. *J. Geophys. Res.* **99,** 19867–19884 (1994).
16. Allègre, C. J. & Turcotte, D. L. Implications of a two-component marble-cake mantle. *Nature* **323,** 123–127 (1986).
17. Sobolev, S. V. & Babeyko, A. Y. Modeling of mineralogical composition, density and elastic-wave velocities in anhydrous magmatic rocks. *Surv. Geophys.* **15,** 515–544 (1994).
18. Snyder, G. A. *et al.* The origins of Yakutian eclogite xenoliths. *J. Petrol.* **38,** 85–113 (1997).
19. Yasuda, A., Fujii, T. & Kurita, K. Melting phase relations of an anhydrous mid-ocean ridge basalt from 3 to 20 GPa: Implications for the behavior of subducted oceanic crust in the mantle. *J. Geophys. Res.* **99,** 9401–9414 (1994).
20. Yaxley, G. M. & Green, D. H. Reactions between eclogite and peridotite: mantle refertilisation by subduction of oceanic crust. *Schweiz. Mineral. Petrogr. Mitt.* **78,** 243–255 (1998).
21. Eiler, J. M., Farley, K. A., Valley, J. W., Hofmann, A. W. & Stolper, E. M. Oxygen isotope constraints on the sources of Hawaiian volcanism. *Earth Planet. Sci. Lett.* **144,** 453–468 (1996).
22. Stakes, D. S. & Taylor, H. P. The northern Samail ophiolite - an oxygen isotope, microprobe, and field-study. *J. Geophys. Res. B* **97,** 7043–7080 (1992).
23. Hart, S. R., Blusztajn, J., Dick, H. J. B., Meyer, P. S. & Muehlenbachs, K. The fingerprint of seawater circulation in a 500-meter section of ocean crust gabbros. *Geochim. Cosmochim. Acta* **63,** 4059–4080 (1999).
24. Hart, S. R. Equilibration during mantle melting - a fractal tree model. *Proc. Natl Acad. Sci. USA* **90,** 11914–11918 (1993).
25. Rhodes, J. M. Geochemistry of the 1984 Mauna Loa eruption - implications for magma storage and supply. *J. Geophys. Res. B* **93,** 4453–4466 (1988).
26. Stolper, E. M., DePaolo, D. J. & Thomas, D. M. Introduction to special section: Hawaii Scientific Drilling Project. *J. Geophys. Res.* **101,** 11593–11598 (1996).
27. Sharp, W. D., Turrin, B. D., Renne, P. R. & Lanphere, M. A. The $^{40}Ar/^{39}Ar$ and K/Ar dating of lavas from the Hilo 1-km core hole, Hawaii Scientific Drilling Project. *J. Geophys. Res.* **101,** 11607–11616 (1996).
28. Roedder, E. Fluid inclusions. *Rev. Mineral* **12,** 1–644 (1984).
29. Danyushevsky L. V., Della-Pasqua, F. N. & Sokolov, S. Re-equilibration of melt inclusions trapped by magnesian olivine phenocrysts from subduction-related magmas: petrological implication. *Contrib. Mineral. Petrol.* **138,** 68–83 (2000).
30. Hofmann, A. W. Chemical differentiation of the Earth: the relationship between mantle, continental crust, and oceanic crust. *Earth Planet. Sci. Lett.* **90,** 297–314 (1988).
31. Garcia, M. O. Petrography, olivine and glass chemistry of lavas from the Hawaii Scientific Drilling Project. *J. Geophys. Res.* **101,** 11701–11713 (1996).

Supplementary Information is available on Nature's World-Wide Web site (http//www.nature.com) or as paper copy from the London editorial office of Nature.

Acknowledgements

We thank the HSDP team for providing samples. We thank S. Simakin for ion probe analyses of inclusions; L.V. Danyushevsky for the access to PETROLOG thermodynamic modelling software; S.V. Sobolev for modelling phase compositions at high T-P; P. Kelemen for providing unpublished data on Oman Gabbro; E. Macsenaere-Riester for help with the electron microprobe analyses; F. Künstler for preparing doubly polished sections; and F. Frey, J. Eiler, L.V. Danuyshevsky, V. S. Kamenetsky, A. A. Gurenko and S. R. Hart for comments that helped to improve the clarity of the manuscript. This work was supported by Deutsche Forschungsgemeinschaft and the Russian Foundation of Basic Research (A.V.S. and I.K.N.) and an Alexander von Humboldt award (A.V.S.).

Correspondence and requests for materials should be addressed to A.V. S. (e-mail: asobolev@mpch-mainz.mpg.de)

Recycled oceanic crust observed in 'ghost plagioclase' within the source of Mauna Loa lavas

Alexander V. Sobolev[*,†], Albrecht W. Hofmann[*] & Igor K. Nikogosian[*,‡,†]

*-Max-Planck-Institut für Chemie, Postfach 3060, 55020 Mainz, Germany
†-Vernadsky Institute of Geochemistry, Russian Academy of Sciences, Kosygin str.19, 117975 Moscow, Russia
‡-Department of Petrology, Vrije Universiteit, De Boelelaan 1085, 1081 HV, Amsterdam, Netherlands

Supplementary Information

Table 1. Composition of Sr-rich and representative "normal" melt inclusions in olivines from Mauna Loa lavas

Sample	H-1	H-1	R129	R129	R129	H-OC	H-OC	H-OC	H-OC	H-OC
Incl	**27**	**II/70**	**28-1c**	**31-1b**	**30/2a**	**76-B**	**76-A**	**76-C**	**76-D**	**76-E**
Type	Sr-r.	Sr-r.	Sr-r.	Sr-r.	Sr-r.	Sr-r.	norm.	norm.	norm.	norm.
Host Ol ol	84.4	87.1	89.8	88.8	85.3	88.6	87.9	89.0	88.1	88.0
Diam	40	45	30	70	50	50	300	50	40	120
Tq	1250	1270	nat.	nat.	nat.	1280	1280	1280	1280	1280
Measured concentrations (wt.%)										
SiO2	51.2	52.4	56.9	56.3	56.5	52.7	51.7	54.5	53.2	51.9
TiO2	1.7	1.9	2.6	1.7	2.2	2.1	2.1	1.7	2.1	2.2
Al2O3	13.4	13.8	17.6	17.7	17.6	13.4	13.2	13.3	13.1	13.3
FeO	11.2	6.8	4.2	4.9	6.0	7.5	10.1	6.5	7.0	8.6
MnO	0.1	0.2	0.1	0.1	0.1	0.1	0.1	0.1	0.1	0.1
MgO	10.0	11.0	2.5	3.1	2.3	10.8	11.5	11.6	11.1	10.6
CaO	8.9	11.0	12.9	13.7	13.7	11.0	10.0	10.1	10.4	10.6
Na2O	2.1	2.2	2.7	2.6	3.1	2.2	1.5	2.4	2.2	2.5
K2O	0.19	0.22	0.24	0.18	0.17	0.16	0.37	0.04	0.28	0.44
P2O5	nd	0.20	0.15	0.17	0.14	0.13	0.17	0.02	0.18	0.24
H2O	0.18	0.26	0.28	0.31	0.33	0.26	0.25	nd	0.31	nd
Corrected for equilibrium with host olivine and assumed original FeO=11.2										
Xol 1	0.000	0.107	0.362	0.324	0.256	0.143	0.071	0.160	0.129	0.109
SiO2	51.2	50.5	50.1	50.3	51.1	50.3	50.3	51.3	50.9	50.0
TiO2	1.7	1.7	1.6	1.2	1.6	1.8	1.9	1.4	1.8	2.0
Al2O3	13.4	12.3	11.2	12.0	13.1	11.5	12.3	11.1	11.4	11.8
FeO	11.2	11.2	11.2	11.2	11.2	11.2	11.2	11.2	11.2	11.2
MnO	0.1	0.1	0.1	0.1	0.1	0.1	0.1	0.1	0.1	0.1
MgO	10.0	11.8	15.4	13.9	10.1	13.5	12.8	14.2	13.0	12.5
CaO	8.9	9.8	8.2	9.3	10.2	9.4	9.3	8.5	9.1	9.4
Na2O	2.1	2.0	1.7	1.8	2.3	1.9	1.4	2.0	1.9	2.2
K2O	0.19	0.20	0.15	0.12	0.13	0.14	0.34	0.03	0.24	0.39
P2O5	nd	0.18	0.10	0.12	0.10	0.11	0.16	0.02	0.16	0.21
H2O	0.18	0.23	0.18	0.21	0.24	0.22	0.23	nd	0.27	nd
Corrected for olivine fractionation to equilibrium with olivine Fo 90.8										
Xol 2	0.181	0.228	0.397	0.389	0.389	0.225	0.178	0.232	0.226	0.207
SiO2	49.7	49.1	49.6	49.4	49.2	49.4	49.2	50.4	49.8	48.9
TiO2	1.4	1.5	1.6	1.0	1.3	1.6	1.7	1.3	1.6	1.8
Al2O3	11.0	10.6	10.6	10.9	10.8	10.4	10.8	10.2	10.1	10.5
FeO	11.3	11.2	11.2	11.2	11.2	11.2	11.2	11.2	11.2	11.2
MnO	0.1	0.1	0.1	0.1	0.1	0.1	0.1	0.1	0.1	0.1
MgO	17.2	16.8	17.1	17.0	16.7	16.8	17.0	17.1	17.0	16.4
CaO	7.3	8.5	7.8	8.5	8.4	8.5	8.2	7.7	8.0	8.4
Na2O	1.7	1.7	1.6	1.6	1.9	1.7	1.3	1.8	1.7	2.0
K2O	0.15	0.17	0.14	0.11	0.10	0.13	0.30	0.03	0.21	0.35
P2O5	nd	0.16	0.10	0.11	0.09	0.10	0.14	0.02	0.14	0.19
H2O	0.15	0.20	0.17	0.19	0.20	0.20	0.21	nd	0.24	nd
Trace elements ppm										
Ba	45	30	19	23	23	25	67	5	39	78
Th	0.14	0.24	0.12	0.15	0.10	0.11	0.46	0.06	0.19	0.42
Nb	1.45	3.87	1.62	2.09	1.87	1.52	7.24	0.54	3.72	9.44
La	5.16	3.25	3.71	3.47	2.58	2.36	8.25	1.32	4.60	7.86
Ce	19.2	9.08	12.4	8.26	6.55	6.86	20.2	5.79	12.6	20.1
Sr	659	344	408	347	389	437	262	52	155	270
Nd	17.9	7.37	10.8	5.95	6.24	7.08	13.1	6.78	9.85	14.1
Zr	86.5	58.8	81.0	34.1	34.0	42.8	102	36.0	67.4	97.5
Sm	4.62	2.49	2.84	1.93	2.72	2.96	3.57	2.87	3.00	3.91
Eu	1.42	0.90	1.04	0.77	1.13	1.11	1.20	0.97	0.98	1.47
Ti	7600	8460	9430	6890	7820	8710	10000	7460	8650	10900
Dy	4.03	3.07	3.23	3.04	3.11	3.23	4.00	2.76	2.92	4.04
Er	1.94	1.61	1.65	1.83	1.73	1.76	2.02	1.68	1.53	2.01
Y	16.4	13.5	16.1	17.5	16.1	18.6	18.9	19.2	17.8	18.1
Yb	1.59	1.39	1.26	1.41	1.54	1.57	1.88	1.49	1.44	1.9

Note to Table 1: The compositions are presented in measured values and two stages of correction (see Methods section in the paper). These values differ only in the weight fraction of olivine added to measured values. This is zero for measured values, Xol1 for the first correction (to bring the melt inclusion to equilibrium with the host olivine and an FeO content of 11.2 %), and Xol 2 for the second fractionation correction (to bring the melt to equilibrium with the most magnesian olivine of the suite of lavas, Fo 90.8). Trace elements are presented only for the final correction stage, because initial values can easily be back-calculated using the amount of added olivine and the assumption that olivine contains no incompatible elements. Host Ol – Forsterite content of host olivine in mole percent; Diam - average inclusion diameter in micrometers; Tq - quenching temperature (in deg. C) for heated melt inclusions; naturally quenched melt inclusions are marked- nat.; Sr-rich - Sr-r.; normal - norm.; nd- not determined.

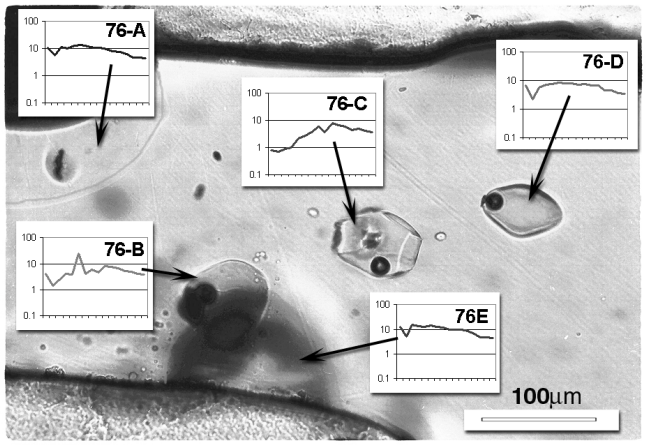

Figure 5. Olivine grain 76 in 1868 Mauna Loa lava (sample H-OC). Five inclusions (76-A to E as in Table 1) are visible in the fragment of olivine grain. 76A is large inclusion covering the entire upper left corner. Incompatible element patterns (as in Figure 2A) are shown for each inclusion. The large shadow under Sr-rich inclusion 76B is a big "normal" inclusion 76E situated around 100 mm below inclusion 76B. Note exceptional diversity of incompatible element compositions of trapped melts on the scale of a few hundred micrometers.

Modeling

All modeling involving crystallization or (and) assimilation was carried out using PETROLOG software[3].

Plagioclase saturation model

Plagioclase of fixed composition was added in small increments (0.01 wt%) to the reconstructed compositions of Sr-rich melts in equilibrium with the host olivine (reconstruction step 2, Table 1, Methods section in the paper). After each increment, the liquidus assemblage of the resulting melt was checked using olivine- melt[4], plagioclase-melt[5] and pyroxene-melt[3] equilibria. The procedure was repeated until plagioclase appeared as an equilibrium phase on the liquidus.

Table 2. Average compositions of melt inclusion groups

Group	normal (143)		Sr-rich (6)		all groups (160)	
	Average	R%	average	R%	Average	R%
SiO_2	49.29	0.7	49.40	0.4	49.26	0.8
TiO_2	1.50	8.9	1.40	14.4	1.50	9.2
Al_2O_3	10.63	2.2	10.73	2.0	10.64	2.3
FeO	11.20	0.3	11.21	0.5	11.20	0.3
MnO	0.07	38.4	0.08	33.5	0.07	38.7
MgO	16.84	1.3	16.91	1.2	16.84	1.2
CaO	8.14	5.2	8.16	5.9	8.13	5.2
Na_2O	1.72	9.2	1.71	7.0	1.72	9.1
K_2O	0.25	18.5	0.13	19.4	0.25	22.6
P_2O_5	0.18	28.9	0.09	55.7	0.20	57.6
Trace elements normalized to PM (A.W. Hofmann, 1988, [ref 1])						
Ba	7.8	22.9	4.6	33.3	7.7	27.2
Th	4.6	25.2	1.8	35.0	4.4	32.1
Nb	9.7	20.0	3.4	44.1	9.5	33.0
K	8.4	18.5	4.4	19.4	8.2	22.6
La	11.2	19.1	5.6	29.1	11.0	22.1
Sr	11.9	15.3	23.7	27.2	12.4	25.2
Ce	10.6	17.3	6.5	46.3	10.5	20.8
Nd	10.0	15.0	7.8	49.8	9.9	17.6
Zr	8.1	11.9	5.8	41.4	8.1	14.7
Sm	8.4	14.8	7.6	31.1	8.3	15.9
Eu	7.1	12.5	7.3	21.2	7.2	13.8
Ti	6.7	8.7	6.3	11.1	6.7	9.0
Dy	5.0	10.7	5.2	11.4	5.0	11.2
Y	4.2	7.4	4.2	10.6	4.2	8.2
Er	4.1	9.0	4.2	6.9	4.1	9.1
Yb	3.6	10.5	3.5	8.8	3.6	10.5

Note to Table 2 R%- standard deviation in % to average value. (160)-number of analyses. All inclusions are corrected to be in equilibrium with Fo 90.8 (see Methods section in the paper). Trace elements are normalized to primitive mantle[1]. Note that HREE and Y for both inclusion groups are similarly depleted and less variable compared to lighter REEs. Actually the variability of HREE is within analytical error. This strongly suggests buffering by garnet in the mantle source of both types of melts[2].

Crustal assimilation modeling

Three models were tested quantitatively in order to check the possibility that high Sr of exotic melt inclusions might be obtained by assimilation of gabbro or plagioclase by "normal" Mauna Loa primary melt without significant change of its major element composition. Results of these models are shown on Fig 4 of the paper. The very Sr rich Gabal Gerf average gabbro[6] was used in order to test the most favorable assimilation scenario.

Model I: Direct assimilation of plagioclase. Plagioclase from Gabal Gerf gabbro (Table 3) was added to the primary normal melt in increments of 5 wt.% until plagioclase saturation was achieved (see previous section and Table 3). The composition of liquidus olivine was calculated using [ref 4] for oxygen fugacity corresponding to quartz-faylite-magnetite buffer[7] and oxidation state of Fe in the melt modeled by the formulation of A.A. Borisov and A.I. Shapkin[8].

Model II: Direct assimilation of gabbro. Similar to model I but average Gabal Gerf gabbro[6] was assimilated instead of plagioclase (see Table 3).

Model III: Assimilation-fractional crystallization process[9]. Gabal Gerf Gabbro was added in increments of 20 wt.% to the "normal primary melt". The amount of crystal fractionation of the resulting melt was emulated using olivine, plagioclase, pyroxene and melt equilibrium formulations[3-5] following each increment of assimilation. The ratio of the rates of fractional crystallization and assimilation was kept fixed in each model. We have varied the extent of fractional crystallization from zero (which corresponds to model II) to 15 %, which brings melt to plagioclase saturation on the first increment. The case shown on Fig. 4 of the paper (model III) corresponds to 5 wt.% of fractional crystallization following each assimilation event and represents the maximum ratio between crystallization and assimilation rates (r=4), which is capable of producing the required enrichment in Sr and Sr/Ce ratio in the melt.

Table 3. Crustal assimilation model

NN	1	2	3	4	5	6	7
SiO2	47.61	54.51	49.26	49.40	51.36	47.94	50.18
TiO2	0.64	0.04	1.50	1.40	0.92	0.81	1.26
Al2O3	20.14	29.28	10.64	10.73	18.10	18.24	17.01
FeO	6.95	0.13	11.20	11.21	6.77	7.80	9.17
MnO	0.10	0.00	0.07	0.08	0.04	0.09	0.12
MgO	8.16	0.00	16.84	16.91	10.11	9.90	8.73
CaO	10.89	11.68	8.13	8.16	9.55	10.34	10.66
Na2O	2.81	5.79	1.72	1.71	3.35	2.59	2.55
K2O	0.17	0.05	0.25	0.13	0.17	0.18	0.24
Trace elements normalized to PM (A.W. Hofmann, 1988, [ref 1])							
Ba	7.98	7.47	7.66	4.56	7.58	7.91	8.66
Th	0.60	0.01	4.38	1.77	2.63	1.35	2.93
Nb	1.16	0.01	9.53	3.35	5.72	2.84	6.32
La	2.30	1.86	11.03	5.57	7.36	4.05	7.82
Sr	30.78	39.68	12.35	23.65	23.28	27.10	23.91
Ce	2.55	2.20	10.51	6.49	7.18	4.14	7.65
Nd	2.28	0.69	9.92	7.75	6.23	3.81	7.15
Zr	1.38	0.01	8.13	5.78	4.88	2.73	5.60
Sm	1.95	0.27	8.34	7.57	5.11	3.23	6.03
Eu	4.12	3.06	7.23	7.29	5.56	4.74	6.53
Ti	2.95	0.24	6.68	6.27	4.10	3.70	5.57
Dy	1.59	0.06	5.04	5.15	3.05	2.28	3.86
Y	1.50	0.05	4.23	4.15	2.56	2.04	3.33
Er	1.35	0.16	4.07	4.21	2.51	1.90	3.16
Yb	1.18	0.02	3.58	3.53	2.15	1.66	2.77

Note to Table 3 (1)-Average Gabal Gerf Gabbro; (2)-plagioclase from sample GG258 of Gabal Gerf Gabbro; (3)-composition of primary melt for normal inclusions; (4)-composition of primary melt for average Sr-rich inclusion; (5)-final result of model I (40% assimilation of plagioclase (composition 2) by the melt (composition 3)); (6)-final result of model II (80% assimilation of gabbro (composition 1) by the melt (composition 3)); (7)- final result of model III (AFC model for assimilation of gabbro (composition 1) by the melt (composition 3) with ratio of assimilation rate to crystallization rate r= 4).

Reactive porous flow model (not shown on Figure).
The reactive porous flow of "normal" Mauna Loa melt through plagioclase bearing materials[10] could also create high Sr concentrations by processing large amounts of plagioclase. However, this model requires plagioclase saturation to be achieved before significant amounts of Sr could be incorporated (G. Suhr, personal communication).

Sample calculation of melting model

Detailed modeling exceeds the scope of the present publication. Here we show only a sample calculation illustrating the fact that a characteristic "ghost plagioclase signature" of Sr-rich inclusions could be transferred from recycled gabbro to the mantle source by small amounts of partial melts. The following section explains our models in detail and Tables 4-6 present input parameters and results of modeling.

Table 4. Phase composition of gabbro and mixed mantle sources after S.V. Sobolev and A.Y. Babeyko (ref 11).

NN	1	2	3	4	5	6
SiO2	47.61	45.96	46.90	47.83	49.71	64.7
TiO2	0.64	0.181	0.31	0.43	0.68	2.7
Al2O3	20.14	4.06	4.59	5.12	6.19	14.7
FeO*	6.95	7.54	7.37	7.21	6.87	4.2
MnO	0.10	0.00	0.00	0.00	0.00	0.0
MgO	8.16	37.78	35.96	34.14	30.50	1.4
CaO	10.89	3.21	3.24	3.28	3.35	3.9
Na2O	2.81	0.33	0.52	0.71	1.09	4.1
K2O	0.17	0	0.18	0.36	0.72	3.6
Mg#	0.677	0.899	0.897	0.894	0.888	0.8
Conditions						
P kbar	50	30	30	30	30	-
T °C	1400	1550	1550	1550	1550	-
Phase proportions						
Ol	0.0	52.8	47.1	41.5	30.3	-
Cpx	38.6	26.4	29.9	33.3	40.3	-
Opx	0.0	14.1	15.9	17.5	19.9	-
Ga	50.9	6.5	5.7	5.0	4.1	-
Co	8.8	0	0	0	0	-
Ky	1.1	0	0	0	0	-
Ru	0.5	0	0	0	0	-

.

Note to Table 4 1 - Gabal Gerf Gabbro[6]; 2 - mantle composition[1]; 3-5 mixed mantle sources produced by mixing of mantle composition (2) with 5, 10 and 20 wt. % of eclogite partial melt (composition 6 after G.M. Yaxley and D.H. Green[12]) respectively.

The melting model consists of 3 steps:

1. Partial melting of eclogite created from recycled crustal component. The crustal component is assumed to be average Gabal Gerf gabbro[6]. The phase composition of eclogite was estimated using this gabbroic major-element composition and the thermodynamic model of S.V. Sobolev and A.Y. Babeyko[11]. The melting mode was taken from the experiments of G.M. Yaxley and D.H. Green[12]. The critical melting model[13] was used. This model assumes that the system melts in the fractional mode after a critical melt fraction has been reached. This constant critical melt fraction (also called residual source porosity) then remains in the residue to prevent compaction and unrealistic depletion of instantaneous melts. At a fixed source composition and melting mode, the trace element composition of this melt will depend on the melt fraction and whether it is an integral or instantaneous melt. In contrast to integral melt, the instantaneous one critically depends on the residual source porosity[13]. Here we present the calculation for both integral and instantaneous melt approximations for residual eclogite porosity of 8%, which seems reasonable for high-Si melts[12].

2. "Fertilization" of mantle source by partial melt from eclogite. As shown by experimental work[12], the melt produced in quartz (coesite) eclogite will react with adjacent peridotite to form zones enriched in pyroxenes. Quantitative modeling[11] of the phase change in the peridotite as a function of the amount of added melt is shown in Table 4. The major element composition of the reacted melt was used after G.M. Yaxley and D.H. Green[12], the trace element composition was modeled as explained in the previous section. As mantle composition we have used a mantle depletion model resulting from extraction of average continental crust[1]. This step produces the mixed mantle source used in step 3.

3. Melting of the mixed mantle source. We use a critical melting model[13] with 2% of residual mantle porosity and integral melt composition. The reasonable extent of melting was assumed to be between 5 and 15 %.

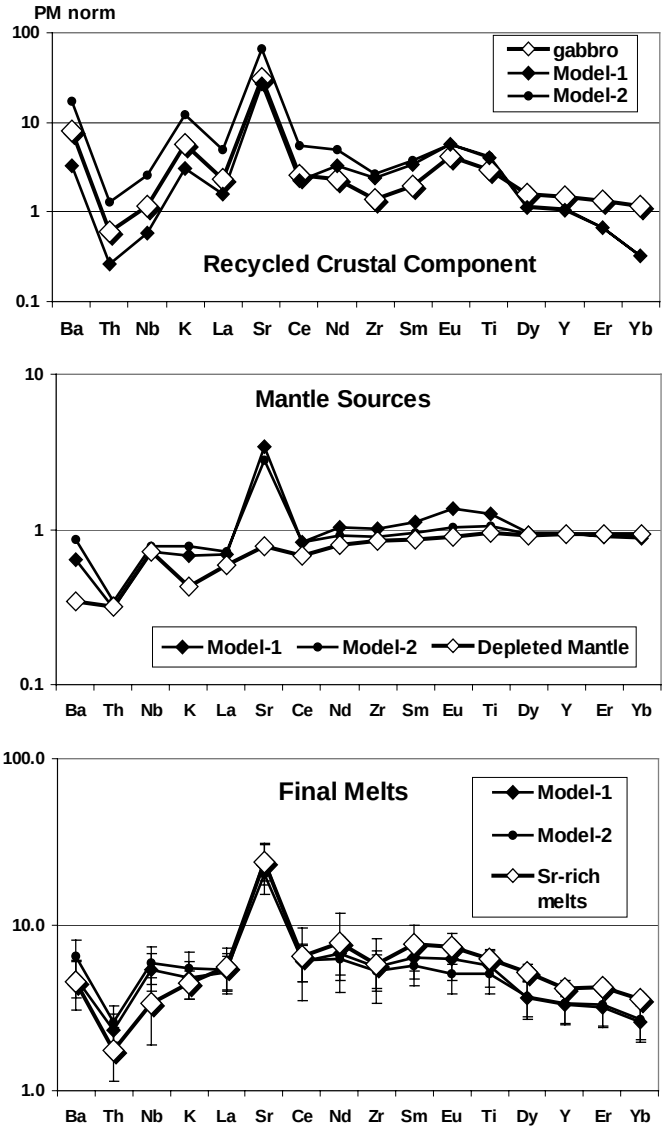

Figure 6. Sample calculation of melting models. Each panel shows the same two models for recycled crustal component, mixed mantle source and final melting products, respectively. Error bars for models correspond to 25% relative. Error bars for Sr-rich melts correspond to one standard deviation (Table 2). See text for explanations.

Two best-fit results are shown on Figure 6 and more results in Table 6. **Model-1** assumes that the mixed mantle source composed of 10 % instantaneous melt (produced by 30% partial melting of eclogite) and 90% depleted mantle component has been melted up to 15%. **Model-2** assumes that the mixed mantle source composed of 3 % integral melt (produced by 50% of partial melting of eclogite) and 97% depleted mantle component has been melted up to 15%.

Both model calculations match Sr-rich melt compositions within 25% relative error for most elements. We do not claim that these solutions are unique, because the number of variables is quite large. However, we do suggest that these solutions are possible. Two important features of the results should be noted:

Table 5. Input parameters for sample calculation of melting model

Composition			Kd solid-melt					
Elements	DM	GAB	OL	OPX	CPX	GA Py84	GAPy60	Co
Ba	2.08	48.25	0.000005	0.000006	0.0003	0.00007	0.00007	0
Th	0.03	0.05	0.000007	0.00002	0.0021	0.011	0.1	0
Nb	0.45	0.72	0.00005	0.003	0.0089	0.03	0.1	0
K	106	1404	0.00002	0.0001	0.1	0.22	0.13	0
La	0.36	1.41	0.0002	0.0031	0.054	0.004	0.17	0
Sr	14.28	561	0.00007	0.0021	0.086	0.012	0.2	0
Ce	1.09	4.09	0.0003	0.0023	0.19	0.09	0.26	0
Nd	0.95	2.71	0.00004	0.0007	0.091	0.002	0.6	0
Zr	8.25	13.42	0.001	0.012	0.26	0.4	3.1	0
Sm	0.34	0.75	0.0009	0.0037	0.27	0.28	0.4	0
Eu	0.13	0.60	0.0005	0.009	0.43	0.5	1.3	0
Ti	1233	3835	0.015	0.086	0.4	0.2	1	0
Dy	0.59	1.01	0.0027	0.011	0.44	1.6	2.1	0
Y	3.68	5.89	0.0082	0.015	0.47	2	2.3	0
Er	0.39	0.56	0.0109	0.021	0.39	2.4	2.4	0
Yb	0.39	0.49	0.024	0.038	0.43	3.3	2.6	0
				Eclogite				
Starting mode			0	0	0.40		0.50	0.1
Melting mode			0	0	0.70		0.00	0.3
				Lherzolite				
Reaction			-1.1	0.4	0.7	0		0
Starting mode			0.530	0.140	0.265	0.065		0
Melting mode			0.1	-0.3	1	0.2		0

Note to Table 5 DM- depleted mantle[1]; Gabbro - average Gabal Gerf gabbro[6]; Kds solid-melt for all minerals except garnet after A.N. Halliday et al[4]. The Kds for quartz (coesite)- melt assumed to be zero. Because it was shown that garnet composition significantly affects its Kds[15], two different Kd sets were used for garnet in the eclogite melting stage (GA Py60) and in lherzolite melting stage (GA Py84), both from ref[15]. (Data for Ce, Nd, Eu and Dy were interpolated from adjacent REEs). OL – olivine; CPX- clinopyroxene; OPX – orthopyroxene; GA – garnet; CO – coesite (quartz).

Table 6. Results of sample calculation of melting model

Model	1	1	1	1	2	2	2	2
Material	EM	MMS	MM	MM	EM	MMS	MM	MM
F (EM)	0.30		-	-	0.50		-	-
X (EM)	-	0.10	-	-		0.03	-	-
F (MMS)	-	-	0.10	0.15	-	-	0.10	0.15
Trace elements normalized to PM (A.W. Hofmann, 1988, ref [1])								
Ba	3.28	0.64	7.68	4.79	17.34	0.85	10.28	6.42
Th	0.26	0.31	3.73	2.33	1.29	0.35	4.15	2.60
Nb	0.59	0.71	8.44	5.35	2.53	0.78	9.26	5.86
K	3.02	0.68	6.44	4.77	12.20	0.78	7.51	5.49
La	1.59	0.69	7.66	5.12	5.00	0.72	8.17	5.39
Sr	26.86	3.39	34.96	24.51	66.82	2.77	29.50	20.25
Ce	2.20	0.83	8.63	6.03	5.54	0.83	8.85	6.06
Nd	3.22	1.04	8.42	6.69	4.90	0.92	7.96	6.17
Zr	2.37	1.00	6.42	5.54	2.69	0.90	6.19	5.27
Sm	3.33	1.12	7.34	6.29	3.74	0.96	6.77	5.70
Eu	5.62	1.37	6.69	6.19	5.78	1.04	5.57	5.10
Ti	4.07	1.26	6.16	5.62	4.20	1.05	5.64	5.08
Dy	1.14	0.94	3.71	3.60	1.15	0.93	3.81	3.68
Y	1.06	0.95	3.36	3.30	1.07	0.94	3.43	3.38
Er	0.66	0.90	3.23	3.18	0.67	0.92	3.32	3.27
Yb	0.33	0.87	2.58	2.60	0.33	0.91	2.68	2.70

Note to Table 6 EM - Eclogite Melt (partial melt from eclogite); MMS - Mixed Mantle Source; MM – Mantle Melt; F (EM)- degree of partial melting of eclogite in wt. fraction; X (EM) - amount of EM in MMS in wt. fraction; F (MMS) - degree of partial melting of MMS in wt. fraction.

(1). Both models require small (10%) to very small (3%) amounts of eclogite partial melt to be introduced to the mixed mantle source. This amount does not affect significantly the phase composition of metasomatized peridotite (see Table 4) and thus will likely not influence the major (compatible) element composition of the final melts. This is also quite clearly demonstrated by the equality of the concentrations of less incompatible elements (Ti, Dy, Y, Er, Yb) between the two models.

(2). The large positive Eu anomaly relative to Sm in the gabbroic component is gradually eliminated in the melting process, and the final result does not show a significant Eu excess relative to Sm. This feature is caused by the presence of garnet in the source materials, which efficiently fractionates Sm from Eu. This could be an explanation also for the absence of Eu excess relative to Sm in the Mauna Loa Sr-rich melts.

1. Hofmann, A. W. Chemical differentiation of the Earth: the relationship between mantle, continental crust, and oceanic crust. *Earth Planet. Sci. Lett.* **90**, 297-314 (1988).
2. Hofmann, A. W., Feigenson, M. D. & Raczek, I. Case Studies On the Origin of Basalt 3. Petrogenesis of the Mauna Ulu Eruption, Kilauea, 1969-1971. *Contributions to Mineralogy and Petrology* **88**, 24-35 (1984).
3. Danyushevsky, L. V. The effect of small amounts of H2O on fractionation of mid-ocean ridge magmas. *EOS Trans. Am. Geophys. Union* **79 suppl.**, S375 (1998).
4. Ford, C. E., Russel, D. G., Craven, J. A. & Fisk, M. R. Olivine-liquid equilibria: Temperature, pressure and composition dependence of crystal/liquid cation partition coefficients for Mg, Fe2+, Ca and Mn. *J. Petrol.* **24**, 256-265 (1983).
5. Ariskin, A. A. & Barmina, G. S. Equilibria thermometry between plagioclases and basalt and andesite magmas. *Geochem. Int.* **27**, 129-134 (1990).
6. Zimmer, M., Kröner, A., Jochum, K. P., Reischmann, T. & Todt, W. The Gabal Gerf complex: A Precambrian N-MORB ophiolite in the Nubian Shield, NE Africa. *Chem. Geol.* **123**, 29-51 (1995).
7. Sobolev, A. V. & Nikogosian, I. K. Petrology of long-lived mantle plume magmatism: Hawaii (Pacific) and Reunion Island (Indian Ocean). *Petrology* **2**, 111-144 (1994).
8. Borisov, A. A. & Shapkin, A. I. New Empiric Equation of Dependence of Fe-3+/Fe-2+ Ratio in Natural Melts On Their Composition, Oxygen Fugacity and Temperature. *Geokhimiya*, 892-897 (1989).
9. Depaolo, D. J. Trace-Element and Isotopic Effects of Combined Wallrock Assimilation and Fractional Crystallization. *Earth and Planetary Science Letters* **53**, 189-202 (1981).
10. Suhr, G. Melt migration under oceanic ridges: Inferences from reactive transport modelling of upper mantle hosted dunites. *Journal of Petrology* **40**, 575-599 (1999).
11. Sobolev, S. V. & Babeyko, A. Y. Modeling of mineralogical composition, density and elastic-wave velocities in anhydrous magmatic rocks. *Surv. Geophys.* **15**, 515-544 (1994).
12. Yaxley, G. M. & Green, D. H. Reactions between eclogite and peridotite: mantle refertilisation by subduction of oceanic crust. *Schweiz. Mineral. Petrogr. Mitt.* **78**, 243-255 (1998).
13. Sobolev, A. V. & Shimizu, N. Ultra-depleted melts and the permeability of oceanic mantle. *Doklady Akademii Nauk* **326**, 354-350 (1992).
14. Halliday, A. N. *et al.* Incompatible Trace-Elements in Oib and Morb and Source Enrichment in the Sub-Oceanic Mantle. *Earth and Planetary Science Letters* **133**, 379-395 (1995).
15. van Westrenen, W., Blundy, J. & Wood, B. Crystal-chemical controls on trace element partitioning between garnet and anhydrous silicate melt. *American Mineralogist* **84**, 838-847 (1999).